最优化 风扇个数n和风扇速度N
使得 qin =qout
产生的热量等于派出的热量

Optimization of an Automotive Radiator Fan Array Operation to Reduce Power Consumption

Tianwei (Thomas) Wang, Amit Jagarwal, John R. Wagner, *Senior Member, IEEE*, and Georges Fadel

Dr Can 风扇矩阵, 优化控制; min cost
控制变量: fan个数 和 speed 的 组合
mixed integer nonlinear programming

***Abstract*—The cooling system for internal combustion engines removes waste heat to ensure a normal in-cylinder combustion process. To accomplish this task, the thermostat valve, radiator, radiator fan(s), and water pump circulate cooling fluid through the engine block and reject heat to the local environment. Since the cooling system consumes a portion of the engine's power, it is important that its operation uses minimal input energy. In this paper, a multiple radiator fan matrix was controlled to minimize energy usage for subsequent efficiency gains. A mathematical model for the radiator fan(s) and the forced convection heat transfer process was developed to establish a mixed integer nonlinear programming problem. An interior points approach was introduced to solve the minimization problem. A series of laboratory tests have been conducted with different fan and speed combinations, with the objective to cool a thermal-loaded engine. Both the mathematical approach and test results indicated similar control strategies. Based on the tests data and accompanying mathematical analysis, an optimization control strategy reduced the fan matrix power consumption by up to 67% for the specified thermal load. An improvement in cooling system performance can offer greater vehicle fuel economy to help meet legislated mobility standards.**

***Index Terms*—Automotive cooling, electro-mechanical actuators, experimental test, radiator fan control, thermal management, optimization.**

I. Introduction

THE cooling system in gasoline and diesel engines serves an important role in maintaining the desired coolant temperature for enhanced performance [1], [2]. If the engine operates too hot, then abnormal in-cylinder combustion may occur leading to degraded fuel economy and tailpipe emissions. Approximately 25% of the total petroleum energy converted during the spark ignition engine combustion process is lost to the cooling system [3]. As a result, the cooling system must accommodate a significant amount of heat while working under ambient operating conditions. The cooling system also consumes a portion of the crankshaft power, so it is important to develop an optimization control method for minimum power consumption by the thermal system actuators. An interesting cooling system configuration is a radiator fan array with distributed actuators under real-time computer control.

A number of research studies have been conducted to investigate the modeling and analysis of advanced vehicle thermal management systems. Mitchell *et al.* [4] examined the role of thermostatic valves in vehicle cooling systems, comparing the performance of various system designs. Chanfreau *et al.* [5] developed a method of controlling fan valves and pump actuators to improve cooling system efficiency. Wagner *et al.* [6] studied the integration of an electrical water pump and an intelligent thermostat valve to achieve faster engine warm-up, reduced temperature fluctuation, and efficient cooling. Page *et al.* [7] investigated a classical proportional-integral-derivative control system featuring multiple electric radiator fans with heat-controlled valves or thermostats. Badekar *et al.* [8] described a microprocessor-based controller for automotive radiator fans to reduce power consumption and to optimize component size. Salah *et al.* [9], [10] designed a nonlinear control strategy for adjusting the smart valve position and the coolant flow speed to track the desired transient temperature. Although these articles focused on automotive thermal management, a radiator fan array with speed control was not examined in the context of power reduction.

track 想要的温度

Forced heat transfer convection, which depends on the size and type of cooling system, may be required in addition to natural (or free) radiator convection. Increased control of the fan motors is possible with electric actuators as they have the potential of making the decoupled fan matrix cooling system energy efficient which may lead to a reduction in engine fuel consumption. In addition, a highly controllable cooling system running on feedback from dynamically acquired sensor data using embedded control algorithms has been shown to help reduce tailpipe emissions [11]. A number of researchers [12]–[14] have investigated numerical and computational fluid dynamics methods to describe the air dynamics within vehicle radiator systems. However, no detailed or validated mathematical model has been published in the open literature which describes the relationship between radiator electric fan matrix operating conditions and the forced convection heat rejected from the radiator.

The optimization of multiple radiator fan(s) speeds to minimize energy usage for certain efficiency gains can impact engine performance. This paper presents a detailed mathematical model to accurately describe the forced convection heat transfer process in internal combustion engines using multiple variable speed radiator fans. Based on this lumped parameter system model, a nonlinear optimization algorithm has been developed to identify the best combination of the electric motor fan operation. In addition, according to a series of designed experimental

Manuscript received May 16, 2014; revised August 26, 2014 and October 31, 2014; accepted November 22, 2014. Date of publication December 23, 2014; date of current version August 24, 2015. Recommended by Technical Editor H. Fujimoto. This work was supported in part by a Sauer-Danfoss Research Grant.

T. Wang, J. R. Wagner, and G. Fadel are with the Mechanical Engineering Department, Clemson University, Clemson, SC 29634 USA (e-mail: tianwew@g.clemson.edu; jwagner@clemson.edu; fgeorge@clemson.edu).

A. Jagarwal is with the TRW Automotive, Rogersville, TN 37857 USA (e-mail: ajagarw@g.clemson.edu).

Color versions of one or more of the figures in this paper are available online at http://ieeexplore.ieee.org.

Digital Object Identifier 10.1109/TMECH.2014.2377655

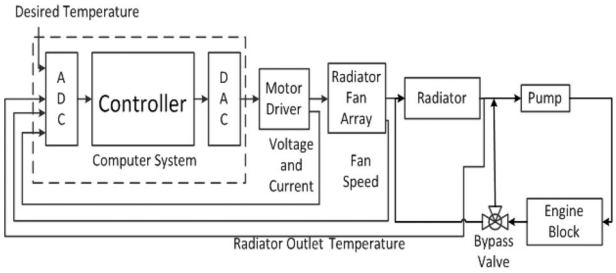

Fig. 1. Block diagram for radiator fan colltroller system.

tests, a general "Rule of Thumb" is proposed for the cooling system operation that does not use a mathematical foundation. The control method contained in this paper establishes a basis for future controller designs.

The remainder of the paper is organized as follows. In Section II, a mathematic model of the prototype cooling system and fan matrix is offered. The optimization problem is introduced and the interior point method applied to solve this problem in Section III. In Section IV, a forced convection cooling system experiment with an electric fan array is created. The test results and engineering analysis of the experiments are presented and discussed in Section V. Finally, the conclusion is offered in Section VI.

II. Mathematical Model

The research objective was to cool an internal combustion engine with a matrix of electric radiator fans to minimize power consumption by selecting different fan combinations and motor speeds. To formulate the optimization problem, the governing equations for the thermal system dynamics are derived for the feedback control diagram in Fig. 1.

In this analysis, a series of seven assumptions may be imposed on the thermal system:

- *A1: No heat losses in the system occur other than forced convection through the radiator.*
- *A2: The heat output from the radiator equals the heat input from the engine at steady-state operation;* $q_{\rm in} = q_{\rm out}$.
- *A3: Ram air effects may need to be considered due to vehicle motion and/or wind.*
- *A4: System temperatures and fluid flows are measured using available sensors.*
- *A5: Coolant flows entirely through the radiator and not the by-pass circuit based on the thermostat.*
- *A6: Water pump operation is fixed so that system heat rejection is based on fan speeds.*
- *A7: Air temperature drop,* ΔT*, across the radiator is a known constant.*

A. Estimation of Heat From Combustion Process

An analytical model for the combustion process generated heat that must be expelled through forced air convection by the radiator fans can be calculated. The heat rejection rate from the engine combustion cylinders to the coolant flowing through the block water jackets, q_c, may be stated [15] as

$$q_c = {\rm UA}_p\,(T_g - T_c) \tag{1}$$

where U is the overall heat transfer coefficient, A_p is the piston head surface area, T_g is the mean effective gas temperature, and T_c is the coolant temperature. For a given engine application, the variable T_g can either be directly measured by an in-cylinder sensor or obtained from table look up based on the air/fuel ratio, spark angle, and load per calibration. In this study, the heat rejection from the combustion process is considered to be the input heat supplied to the engine block by an external heat exchanger custom designed for the laboratory test.

The heat supplied to the cooling system, $q_{\rm in}$, is based on the low pressure (LP) steam heat exchanger temperature for the experimental laboratory system, which can be expressed as

$$q_{\rm in} = \dot{m}_c Cp_{\rm cool}(T_{\rm HI} - T_{\rm HO}) \tag{2}$$

where $\dot{m}_c$ is the coolant mass flow rate due to the pump, $Cp_{\rm cool}$ is the specific heat of the coolant at constant pressure, and $T_{\rm HI}$ and $T_{\rm HO}$ are the heat exchanger inlet and outlet temperatures, respectively.

B. Heat Rejected From Radiator and Ram Air Effect

To minimize the power consumed by the radiator fan(s), the heat rejected by forced convection must be adjusted through fan motor speed control. The rate of heat rejection from the radiator, $q_{\rm out}$, can be expressed as

$$q_{\rm out} = \varepsilon \dot{m}_{\rm air} Cp_{\rm air}\,(T_{a\rm out} - T_{a\rm in}) \tag{3}$$

where $T_{a\rm out}$ is the air temperature exiting the radiator, $T_{a\rm in}$ is the air temperature at the radiator inlet, and $Cp_{\rm air}$ is the specific heat of the air. The radiator heat transfer efficiency, $0 < \varepsilon < 1$, depends on the air mass flow rate. In this analysis, a quadratic relationship $\varepsilon = a\dot{m}_{\rm air}^2 + b\dot{m}_{\rm air} + c$ was selected where a, b and c are constants [16]. Please refer to the Appendix for the selection of the a, b and c values.

The variable $\dot{m}_{\rm air}$ denotes the air mass flow rate through the radiator and may be calculated as

$$\dot{m}_{\rm air} = Q_{\rm air}\rho_{\rm air} = v_{\rm air}A_r\rho_{\rm air} \tag{4}$$

where $Q_{\rm air} = \dot{m}_{\rm air}/\rho_{\rm air}$ is the volume flow rate, A_r is the radiator area, $\rho_{\rm air}$ is the air density, and $v_{\rm air}$ is the air flow velocity through the radiator. This velocity is a combination of two different sources—the radiator fan(s), and the ram air effect. The total air flow velocity, although complex, can be simplified as

$$K_r v_{\rm air}^2 = K_I v_{\rm ram}^2 + K_f v_f^2 \tag{5}$$

where $K_r, K_I,$ and K_f are the pressure coefficients at the radiator, air inlet, and fan, respectively, as indicated in Fig. 2.

The expression (5) may be rewritten to calculate the air velocity through the radiator as

$$v_{\rm air} = \sqrt{\frac{K_I}{K_r}v_{\rm ram}^2 + \frac{K_f}{K_r}v_f^2}. \tag{6}$$

The volume flow rate, $Q_{\rm air}$, and mass flow rate, $\dot{m}_{\rm air}$, in (4) can now be rewritten as

$$\begin{aligned}\dot{m}_{\rm air} &= \rho_{\rm air}\sqrt{\frac{K_I}{K_r}v_{\rm ram}^2A_r^2 + \frac{K_f}{K_r}v_f^2A_r^2}\\ &= \rho_{\rm air}\sqrt{\frac{K_I}{K_r}Q_{\rm ram}^2 + \frac{K_f}{K_r}Q_f^2}\end{aligned}$$

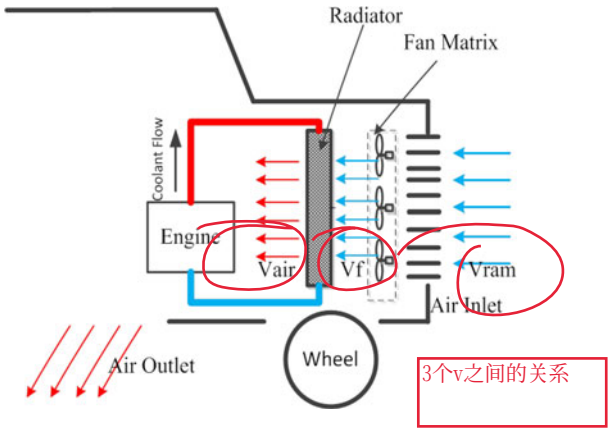

Fig. 2. Simplified air flow circuit (side view of vehicle).

$$= \sqrt{\frac{K_I}{K_r}\dot{m}_{\text{ram}}^2 + \frac{K_f}{K_r}\dot{m}_f^2} \tag{7}$$

where $Q_{\text{ram}} = v_{\text{ram}} A_r$ and $Q_f = v_f A_r$ are the volume flow rates caused by the ram air effect and fan matrix, respectively. The variables $\dot{m}_{\text{ram}} = Q_{\text{ram}} \rho_{\text{air}}$ and $\dot{m}_f = Q_f \rho_{\text{air}}$ denote the ram air and fan air mass flow rates. To obtain the general function for system heat rejection, (3) may now be rewritten as

$$q_{\text{out}} = \varepsilon \left(\sqrt{\frac{K_I}{K_r}\dot{m}_{\text{ram}}^2 + \frac{K_f}{K_r}\dot{m}_f^2} \right) Cp_{\text{air}} \left(T_{a\text{out}} - T_{a\text{in}}\right). \tag{8}$$

C. Fan Laws and Power Consumption

The relationship between the electrical power and fan matrix configuration (fan speed and fan number) must be derived to form the objective equation. The nonlinear function between the fan torque, τ, and the motor speed, N, may be expressed [17] as

$$\tau = kN^2 \tag{9}$$

where the factor k for fans depends on the blade design and its characteristic curve. However, the factor k tends to be typically independent of the motor. As a result, the electrical power, P_e, of the fan with speed N may be determined by introducing the efficiency, η, which is the ratio between the mechanical output power and the electrical input power so that

$$P_e = \frac{P_m}{\eta} = \frac{\tau\omega}{\eta} = \frac{2\pi k}{60\eta} N^3. \tag{10}$$

In this expression, P_m is the mechanical output power. As an alternative, the electrical power can also be determined as $P_e = iV_s$, where i is the current and V_s is the supply voltage.

Further justification for this relationship is based on the fan laws [18] given by

$$\frac{P_1}{P_2} = \left(\frac{N_1}{N_2}\right)^3 \cdot \left(\frac{d_1}{d_2}\right)^5 \cdot \left(\frac{\rho_1}{\rho_2}\right). \tag{11}$$

In other words, the mechanical power can be directly related to the cube of the speed when the diameter and density are constant.

The efficiency, η, of the mechanical output to electrical input power may be represented as a polynomial function of the motor speed, N, assuming an uniform load. In this research, a quadratic expression has been considered whose general form may be expressed as

$$\eta = dN^2 + eN + f \tag{12}$$

where d, e, and f are constants. The methodology to the select the values of d, e, and f are provided in the Appendix. Using this relationship, (10) may now be rewritten as

$$P_e = \frac{2\pi k}{60(dN^2 + eN + f)} N^3. \tag{13}$$

The volume flow rate, Q_f, through a single fan can also determine the required fan motor speed. The speed for a single axial fan to generate a target volume flow rate may be stated as

$$N = \frac{60 Q_f}{4\pi^2 r_m^3 \Phi_m} \left(\frac{1+v^2}{1-v^2}\right) \tag{14}$$

where r_m is the mean radius, v is the hub ratio, and Φ_m is the flow rate coefficient.

The fan air mass flow rate, $\underset{f}{m}$, can be determined by rewriting this expression as

$$m_f = \frac{4\pi^2 \rho_{\text{air}} r_m^3 \Phi_m N n}{60} \left(\frac{1-v^2}{1+v^2}\right). \tag{15}$$

n为同时运行的fan的个数

The integer variable n was introduced to denote the number of operating fans in parallel in the radiator configuration. The mean radius, r_m, is dependent on the fan tip and hub radius, r_t and r_h, such that

$$r_m = \sqrt{\frac{1}{2}(r_t^2 + r_h^2)}. \tag{16}$$

Similarly, the hub ratio,, may be calculated as

$$v = r_h / r_t. \tag{17}$$

Finally, the flow rate coefficient, Φ_{m}, may be obtained for axial flow fans using specific speed and pitch cord ratios [18].

Based on the analysis, substitute (15) into (8), the general function for system heat rejection may be rewritten as

$$q_{\text{out}} = \varepsilon \sqrt{\frac{K_I}{K_r}\dot{m}_{\text{ram}}^2 + \frac{K_f}{K_r}\left(\frac{4\pi^2 \rho_{\text{air}} r_m^3 \Phi_m N n}{60}\left(\frac{1-v^2}{1+v^2}\right)\right)^2} \times Cp_{\text{air}} \left(T_{a\text{out}} - T_{a\text{in}}\right). \tag{18}$$

In this paper, no ram air effects are considered which leads to $\dot{m}_{\text{ram}} = 0$, and corresponds to a stationery engine scenario. The application for this case may be a parked vehicle without blowing wind (e.g., silent sentry mode) or an engine-based generator. Thus, (18) can be expressed as

$$q_{\text{out}} = \varepsilon \frac{4\pi^2 \rho_{\text{air}} r_m^3 \Phi_m N n}{60}\left(\frac{1-v^2}{1+v^2}\right) \times \sqrt{\frac{K_f}{K_r}} Cp_{\text{air}} \left(T_{a\text{out}} - T_{a\text{in}}\right). \tag{19}$$

Refer to Appendix B for the details regarding the mathematical model validation efforts.

III. Optimization Problem

The theoretical relationship between the fan power consumption and the heat rejected for various fan configurations and fan(s) speeds has been derived. Now an optimization problem is formulated and applied to solve this smart cooling system challenge for power minimization which meets heat transfer demands.

A. Problem Description

The governing system dynamics stated in (13) and (19) are well suited for a mixed integer nonlinear programming (MINP) which may be expressed as

$$\min f(N,n) \tag{20a}$$

$$\text{subject to}: \; h(N,n)=0 \tag{20b}$$

$$g(N,n)\le 0 \tag{20c}$$

where N and integer n are programming variables. The objective function, $\mathrm{f}(.,.)$, may be stated as

$$f(N,n)=P_e=\frac{2\pi k}{60(dN^2+eN+f)}nN^3. \tag{21}$$

For (20b) and (20c), the equality and inequality constraints $\mathrm{h}(\mathrm{N},\mathrm{n})=0$ and $\mathrm{g}(\mathrm{N},\mathrm{n})\le 0$ and $g(N,n)$ can be described as

$$h(N,n)=q_{\text{out}}-q_{\text{in}}=\varepsilon\frac{4\pi^2\rho_{\text{air}}r_m^3\Phi_m Nn}{60}\left(\frac{1-v^2}{1+v^2}\right)\times\sqrt{\frac{K_f}{K_r}}Cp_{\text{air}}\left(T_{a\text{out}}-T_{a\text{in}}\right)-q_{\text{in}} \tag{22}$$

$$g(N,n)=\begin{cases}N_{\text{low}}\le N\le N_{\text{high}}\\ 1\le n\le n_{\max}\end{cases} \tag{23}$$

where N_{low}, N_{high}, and $n_{\max}$ denote the lower and upper fan speeds plus the maximum number of operating fans.

The notation in (21) and (22) may be simplified by defining two constants $g$and h where $g=\frac{2\pi k}{60}$ and $h=\frac{4\pi^2\rho_{\text{air}}r_m^3\Phi_m}{60}\sqrt{\frac{K_f}{K_r}}\left(\frac{1-v^2}{1+v^2}\right)Cp_{\text{air}}$. In addition, let $\Delta T=T_{a\text{out}}-T_{a\text{in}}$ correspond to the air temperature drop across the radiator.

The objective function and equality constraint of (21) and (22) may now be expressed as

$$f(N,n)=\frac{g}{(dN^2+eN+f)}nN^3 \tag{24}$$

$$h(N,n)=\varepsilon hNn\Delta T-q_{\text{in}}. \tag{25}$$

The value of ΔT (approximately10 °C → 20 °C) does not significantly affect the optimization results if assumed to be a user-specified constant. In this analysis, all the fans were assumed to have uniform rotational speeds.

B. Optimal Solution to Radiator Fan Consumption

To solve this MINP problem, a related nonlinear constrained programming problem is introduced to determine successive solutions, (N_s,n_s). With the Matlab optimization package, the successive solutions may be first calculated. The function "*fmincon*" provides various types of algorithms; the interior-point approach to constrained minimization was selected to solve a sequence of nonlinear programming minimization problems (refer to [19] and [20] for more details).

The gradient of the objective function,$f(.,.)$, in (24) may be expressed as

$$\nabla f=\left[\frac{\partial f}{\partial N},\frac{\partial f}{\partial n}\right]=\left[\frac{\left(dN^2+2eN+3f\right)gnN^2}{(dN^2+eN+f)^2},\frac{gN^3}{(dN^2+eN+f)}\right] \tag{26}$$

which establishes the search direction for the optimization algorithm. To obtain an integer value for the number of fans,n, per given heat load, q_{out}, the system calculates the two nearest points around the successive solution, (N_s,n_s). The point that does not satisfy the stated constraints is dropped. If both of the two points both satisfy the constraints, then the objective function is calculated based on each point. The point which leads to the smallest objective function value is selected as the best solution.

IV. Experimental System

A test bench was created to provide a safe and repeatable approach for studying automotive engine cooling systems. The experimental station features a wind tunnel and complete set of thermal actuators (variable speed pump, smart valve, and radiator with electric fans) and assorted sensors. A 6.8-L international truck V8 diesel engine with controller area network (CAN) bus controlled the 3×2 fan matrix. Fig. 3 shows the overall system design which also features a steam drive heat exchanger to mimic the internal combustion engine in-cylinder thermal source while creating a test environment for exact heat situation.

A. Heat Source (Steam Supply)

In this experimental bench, an LP steam source simulates the heat generated by the engine. The steam transfers through a multipass heat exchanger to the coolant system which then circulates through the conventional automotive cooling system. Safety equipment such as a pressure regulator, pressure gauge, and safety valve were inserted into the steam system. In this project, the flow rate of the LP steam was constant.

B. Coolant Flow Circuit

The coolant flow circuit consisted of an LP heat exchanger, engine cooling jacket, bypass valve, variable speed coolant pump, and radiator with fan matrix. The coolant received heat from the steam in the multipass heat exchanger and then was pumped into the engine block cooling jacket. From the outlet of the engine cooling jacket, the coolant flows into the directional control valve which, according to the computer-based set point temperature, diverts the coolant back into the engine heat exchanger or lets it flow to the radiator. The variable speed coolant

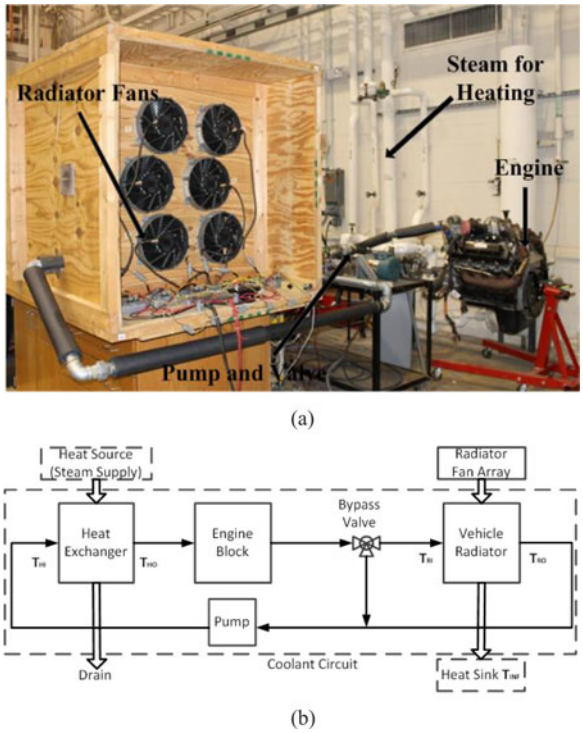

Fig. 3. (a) Picture of experimental testing bench. (b) System block diagram showing main test bench components for radiator fan array testing.

pump was driven by an AC motor controlled by the computer algorithm.

For this study, the DC motor thermostat direct all fluid through the radiator. The coolant enters the radiator from the top inlet port and flows through a mesh of tubes with attached fins, expelling its heat energy to the ambient surroundings. The fluid exits through an outlet in the bottom portion of the radiator into the centrifugal pump. The pump circulates it back to the steam heat exchanger, thus completing the cycle. Insulated galvanized pipes and pipe connections were used to transport the coolant between the various system components.

C. Wind Tunnel

A wind tunnel was constructed to measure the air flow and pressure drop across the radiator on the experimental bench. The wind tunnel has a rectangle matrix arrangement with six fans arranged in three rows and two columns. Each of the fans was connected to a CAN-based DC motor controller; the controllers were connected to be CAN card plugged in the computer PCI port. The fan motors are EMP Fil-11 electric with 24-V brushless DC motors and 600-W rating power. According to experimental motor results, the relationship between efficiency and speed in (14) has been concluded.

D. Sensors, Data Acquisition, and Computer Interface

The experimental bench contained electrical, electronic, and computer subsystems to acquire, process, record, and display data generated during the test runs. Fig. 4 shows the data flow

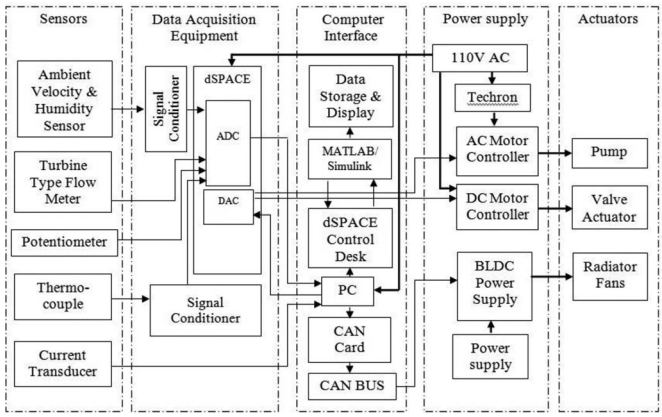

Fig. 4. Block diagram for data flow among the sensors, data acquisition equipment, computer interface, and actuators.

TABLE I
SUMMARY OF SYSTEM MODEL PARAMETERS

Symbol	Value	Units	Symbol	Value	Units
A_r	1.1	m^2	$\dot{m}_c$	1.1	kg/s
a	0.0029	$(s/kg)^2$	n_{max}	6	-
b	−0.072	s/kg	N_{high}	5000	r/min
c	0.86	-	N_{low}	1000	r/min
Cp_{air}	1	kJ/kg•K	r_t	0.14	m
Cp_{cool}	4.18	kJ/kg•K	r_h	0.056	m
d	−5.6e − 8	$(min/rev)^2$	T_{ain}, T_{inf}	293.5	K
e	5.3e − 4	min/rev	ΔT	18	K
f	−0.38	–	ρ_{air}	1.1	kg/m^3
$(K_f/K_r)^{0.5}$	0.78	–	v	0.4	–
k	4.03e − 11	–	Φ_m	0.85	–

path. The sensors used in this experiment included an air speed sensor, a turbine type flow meter, a linear variable differential transducer, five thermocouples, and an ammeter.

The continuous analog data were then supplied to the dSPACE data acquisition system. The computer interface included the software programs MATLAB/Simulink with the vehicle network tool box, and dSPACE. The signal inputs were received through the dSPACE hardware board, while the output control signals were transmitted via the dSPACE DAC and the CAN bus controller.

V. Test Results and Discussion

A series of six tests (varies fan configurations and operating scenarios) were experimentally investigated to study system heat rejection and radiator fan power consumption. The corresponding numerical optimization results were compared with these test results to evaluate the prescribed operating strategy. The system model parameters are listed in Table I for the optimization problem. In this section, the optimization results are presented and discussed.

A. Fan Matrix and Speed Configuration

The coolant flow direction through radiator is shown in Fig. 5 for test configuration #1. The figure indicates that the hottest

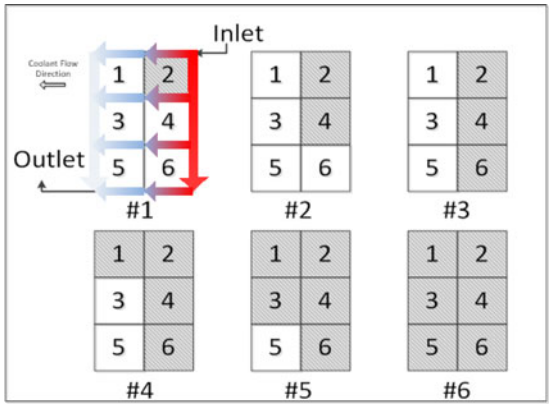

Fig. 5. Fan selection (shaded) at different speeds for six test configurations (I–VI), the color arrows show the coolant temperature trend through the radiator.

TABLE II
SIX FAN MATRIX AND ELECTRIC MOTOR SPEED COMBINATIONS FOR THE EXPERIMENTAL TESTS

Test Set No.	Heat Exchanger Outlet Temp. T_{HO} (°C)	Ambient Temp. T_{ain}, T_{inf} (°C)	Coolant Flow Rate $\dot{m}_c$ (kg/s)	Fan Speed Range, N, (r/min)	Operating Radiator Fans 1 2 3 4 5 6
I	78–81	22			•
II	79–82	24			• •
III	79–81	22		1000 to	• • •
IV	78–81	23	1.1	5000 in	• • • •
V	79–82	23		1000	• • • • •
VI	78–81	23		increments	• • • • • •

area of the radiator is right behind fan no. 2 which correspond to the radiator inlet location, similarly, the region behind fans no. 2, 4, 6 are hotter than that behind fans no. 1, 3, 5. Based on this phenomenon, a design of experiment can be considered as follows, six various fan combinations were designed to evaluate the fan effect. The fan combinations based on experimental observation and fluid flow inlet condition were selected as shown in Fig. 5 and the respective operational speeds as listed in Table II. The fan(s) were connected and controlled by the CAN bus based on the control strategy.

B. Fan Power Consumption

The fan(s) motors voltage, V_s, and the current, i, were used to calculate the power consumption, $P_e = iV_s$. The steady-state dc power consumption values were measured and calculated for the given fan number and operating fan(s) speeds. This fan power consumption data was essential in determining the energy usage for the cooling system for a given engine heat load. Fig. 6 displays the plot of the fan(s) motor electrical power consumption, P_e, for the various fan number,n, with the fan(s) motor speeds, N. This graph indicates the general trend that the increased power consumption is dependent on the number of fans and operating speeds. However, there were exceptions observed at 3000 r/min for the single fan (Test I) and for the five fans (Test V) combinations. In these two cases, the power

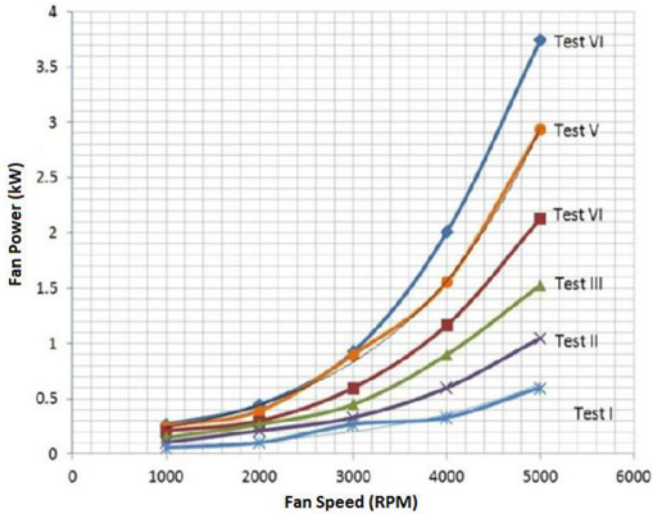

Fig. 6. Fan motor power consumption, P_e, for various fan configurations and fan speeds, N, based on experimental tests to validate the nonlinear releationship between fan speed and power consumption.

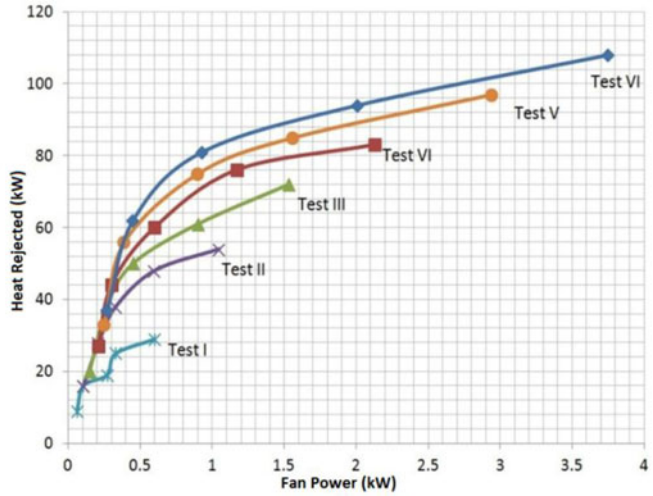

Fig. 7. Fan power, P_e, versus heat rejection, q_{out}, at various fan and speed configurations based on experimental tests.

consumption increased. The power consumption was observed to be almost equal for speeds up to 3000 r/min when either five (Test V) or six (Test VI) fan motors operated. However, all the fan motor combinations have a comparatively smaller variation in power consumption for motor speeds up to 2000 r/min. According to [21], mechanical fans consume 24 to 50 kW of engine power to operate. In comparison, radiator electric fans require approximately 0.7 kW which offer significant energy saving itself.

C. Fan Matrix Performance

The heat rejected versus fan power at various fan speed and fan numbers has been displayed in Fig. 7 over a $0 < P_e < 4$ kW operating range. The graphs represent four parameters;

TABLE III
RULE OF THUMB COMBINATION FOR HEAT REJECTION AND FAN POWER

Heat Rejected, q_{out} (kW)	Fan Number, n	Fan Speed, N (r/min)	Fan Power, P_e (kW)
0–16	1	1000–2000	0–0.10
16–24	2	1000	0.10–0.18
24–35	3	1000	0.18–0.23
35–43	4	1000–2000	0.23–0.30
43–56	5	2000	0.30–0.39
56+	6	2000+	0.39+

heat rejected, q_{out}, fan speed, N, fan number, n, and the fan electric power consumption, P_e. The rejected heat is considered as the objective system input, and then both the fan number and the fan(s) speeds were selected to achieve the heat rejection requirement. This graph should offer guidance in selecting the best energy efficient fan number and speed for a given heat load. The odd point in Test I at heat rejected on 20 kW and fan power at 0.28 may be attributed to diversity of different fans model.

D. Discussion of Experimental Results

The data obtained from the experiments indicated that reduced energy consumption can be achieved for heat rejection rates above $q_{\text{out}} > 56$ kW using all six fan operating configuration. However, when heat rejection need below 56 kW, other fan configurations were observed to be more energy efficient. For example, a heat rejection rate of 48 kW shows Test V with a fan matrix power consumption of $P_e = 0.30$ kW while Test VI was 0.33 kW. For heat rejection in the zone $0 < q_{\text{out}} < 16$ kW, Test I operated in the range of $1000 \leq N \leq 2000$ r/min. Next, the zone of $16 < q_{\text{out}} < 24$ kW and $24 < q_{\text{out}} < 35$ kW corresponds to Test II and III at $N = 1000$ r/min, respectively. If $35 < q_{\text{out}} < 43$ kW, then the Test IV should operate at $1000 \leq \text{N} \leq 2000$ r/min. Finally, $43 < q_{\text{out}} < 56$ kW and $q_{\text{out}} > 56$ kW results in Test V and Test VI at $N = 2000$ r/min, respectively.

E. Rule of Thumb and Numerical Optimization Control Strategy

According to the experimental results show in Fig. 7, a general rule of thumb can be formulated. For heat rejection between 0–56 kW, first start with a single fan (Test I) and operate at $N = 1000$ to 2000 r/min. If more heat rejection is needed, then bring another fan online (Test II–V) till all the six fans (Test VI) operate at $N = 1000$ r/min (perhaps 2000 r/min if needed). Above a heat rejection threshold of 56 kW, use all six fans and increase the fan speed as needed to 5000 r/min. Table III shows the best combination for experimental heat rejection and power configuration with the heat rejection below 56 kW.

The numerical optimization strategy offers an alternative approach to the rule of thumb. Fig. 8 shows the theoretical relationship between the fan power and heat rejection for various configurations and speeds based on Section II. Notice the similarity of the experimental and theoretical curves in Figs. 7 and 8. It suggests the similar trends which demonstrated that the mathematical model is valid.

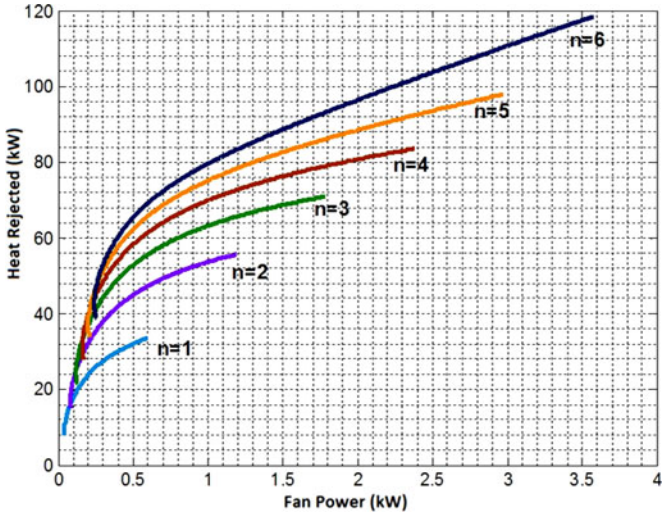

Fig. 8. Theoretical relationship between the fan power, P_e, and heat rejection, q_{out}, at various fan configurations ($n = 1$–6) and speeds.

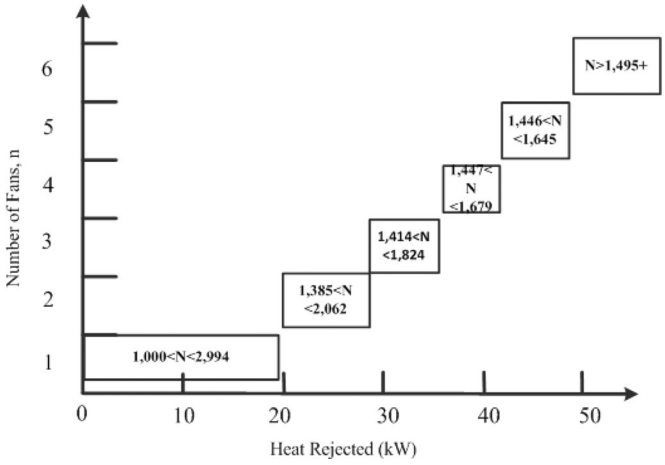

Fig. 9. Optimization control strategy for the fan number, n, heat rejection, q_{out}, and corresponding fan speed, N.

Using an interior-point approach to solve the nonlinear optimization problem, the optimization results are calculated and displayed in Fig. 9 for the ideal selection of fan number, n, and fan(s) speeds, N to achieve specific heat rejection. Representative results are listed in Table IV. According to Fig. 9 and Table IV, an optimization control strategy can be concluded. First, turn on a single fan with its speed at $N = 1000$ r/min, and increase the speed to achieve the increasing heat rejection requirement. Second, turn on the other fans one by one and adjust the corresponding fan(s) speeds. It can be easily demonstrated that this method is similar to the rule of thumb based on the experiments results in Table III.

To illustrate the concept, two specific case studies are considered. In the first case, $q_{\text{out}} = 30$ kW is selected as the heat rejection. The power fan consumption is $P_e = 0.6$ kW for experimental results verses $P_e = 0.51$ kW for the theoretical results

TABLE IV
OPTIMIZATION PROBLEM SOLUTIONS FOR THE RADIATOR FAN ARRAY

Heat Rejected, q_{out}, (kW)	Number of Fans, n	Fan Speed, N (r/min)	Fan Power, P_e (kW)
0–19	1	1000–2994	0–0.09
20–28	2	1385–2062	0.09–0.13
29–36	3	1414–1824	0.14–0.18
37–42	4	1447–1679	0.19–0.22
42–48	5	1446–1645	0.23–0.26
49+	6	1495+	0.27+

TABLE V
CASE STUDY—FAN POWER CONSUMPTION, P_e, FOR DIFFERENT FAN COMBINATIONS

		Pe (kW) theoretical, experimental		
Case	Heat Rejected, q_{out} (kW)	Fan No. $n = 1$	Fan No. $n = 3$	Fan No. $n = 6$
1	30	0.60, 0.51	0.20, 0.16	NA
2	60	NA	0.90, 0.81	0.40, 0.38

when a single fan operates. For the optimization control method, the minimum consumption will reduce to $P_e = 0.2$ kW for experimental result ($P_e = 0.16$ kW for theoretical result) when $n = 3$ fans are operated. In this case, the energy saving is up to 67%. In case 2, the heat rejection selected is $q_{\text{out}} = 60$ kW. Fan number $n = 3$ is selected as the comparison with the optimization result. It indicates that the power consumption is $P_e = 0.9$ kW for experimental results ($P_e = 0.81$ kW for theoretical results) when $n = 3$ fans operate. On the other hand, based on the optimization result, the minimum consumption is approximately $P_e = 0.4$ kW for experimental result ($P_e = 0.38$ kW for theoretical result) when $n = 6$ fans are engaged. The total energy saving corresponds to 55%. For these studies, corresponding fan power consumption for both experimental and theoretical result are shown in Table V.

VI. CONCLUSION

An optimization control method for automotive thermal-management systems can have a positive impact on the cooling system. This paper has studied and analyzed a multiple electric fan radiator cooling configuration using an experimental bench and offline mathematic analysis. According to the experiment and simulation results, a rule of thumb and optimization control strategy were introduced which can reduce the fan matrix power consumption for the specified cooling load. In this study, the power consumption was reduced by approximately 67%.

The methodology proposed in this paper can be used for different radiator fan configurations and heat exchanger sizes to establish operating regime calibrations. The mathematical model can also be used to develop nonlinear control strategies in future work. For instance, a nonlinear controller is under development based on this paper's result to regulate the engines working temperature to a precise temperature range.

TABLE AI
HEAT TRANSFER EFFICIENCY, ε, VERSUS MASS AIR FLOW RATE, $\dot{m}_{\text{air}}$ AT DIFFERENT HEAT REJECTION AND FAN COMBINATIONS

Fan Speed, N (r/min)	Number of Fans, n	Heat Rejected, q_{out}, (kW)	Mass Flow Rate, $\dot{m}_{\text{air}}$ (kg/s)	Heat transfer effectiveness, ε
1000	1	9	0.46	0.978
2000		16	0.92	0.87
3000		19	1.38	0.688
4000		25	1.84	0.679
5000		29	2.3	0.63
1000	2	16	0.92	0.87
2000		28	1.84	0.761
3000		38	2.76	0.688
4000		48	3.68	0.652
5000		54	4.6	0.587
1000	3	20	1.38	0.725
2000		38	2.76	0.688
3000		50	4.14	0.604
4000		61	5.52	0.553
5000		72	6.9	0.522
1000	4	27	1.84	0.734
2000		44	3.68	0.598
3000		60	5.52	0.543
4000		76	7.36	0.516
5000		83	9.2	0.451
1000	5	33	2.3	0.717
2000		56	4.6	0.609
3000		75	6.9	0.543
4000		85	9.2	0.462
5000		97	11.5	0.422
1000	6	37	2.76	0.67
2000		62	5.52	0.562
3000		81	8.28	0.489
4000		94	11.04	0.426
5000		108	13.8	0.391

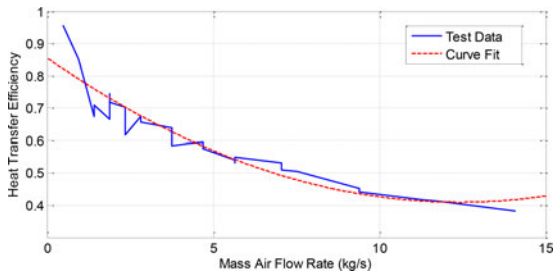

Fig. A.1. Heat transfer efficiency, ε, versus different mass air flow rate, $\dot{m}_{\text{air}}$.

If the optimization algorithm, or a simplified minimization strategy, is constrained by microprocessor speed, then a real-time system can be realized based on table look-ups from either the optimization findings or the "Rule of Thumb" derived from the experimental test results. To further extend the research achievement, the optimization control strategy can also be applied to other transportation applications such as battery pack and electric motor cooling in hybrid powertrain.

APPENDIX A

In this Appendix, the methodologies to select the heat transfer efficiency, ε, and efficiency, η, constants will be presented. Table AI summarizes the experimental measured data including the fan speed, N, air flow rate, $\dot{m}_{\text{air}}$, and the calculated heat rejected,

TABLE AII
EFFICIENCY, η, VERSUS DIFFERENT FAN SPEED, N

Fan Speed, N (r/min)	1000	2000	3000	4000	5000
Fan Power, P_e (kW)	0.05	0.08	0.16	0.31	0.56
Efficiency,η	0.1	0.47	0.72	0.85	0.9

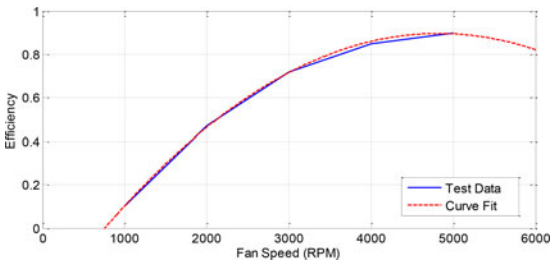

Fig. A.2. Efficiency, η, versus different fan speed, N, combinations.

TABLE BI
MATHEMATICAL MODEL VALIDATION TEST PROFILE WITH FANS NO. 1 AND NO. 2 OPERATED

	Air Mass Flow Rate, $\dot{m}_{\rm air}$, (kg/s)		Heat Rejected, $q_{\rm out}$, (kW)		Power Consumption, P_e, (kW)	
Fan Speed (r/min)	Model Result	Test Result	Model Result	Test Result	Model Result	Test Result
1000	0.92	0.81	15.0	17.3	0.08	0.10
2000	1.84	1.61	27.8	25.0	0.14	0.19
3000	2.76	2.69	38.6	37.0	0.31	0.33
4000	3.68	3.66	47.8	41.8	0.62	0.60
5000	4.60	4.59	55.6	54.8	1.16	1.05
Absolute Average Error %	6.2%		8.9%		11.9%	

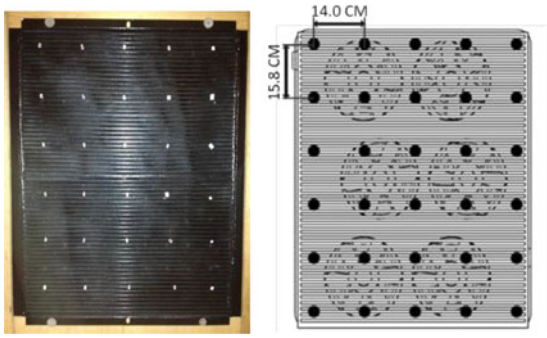

Fig. B.1. Selected points on the radiator frontal area used to measure air velocity.

$q_{\rm out}$, based on the relationship

$$q_{\rm out} = \dot{m}_c C p_{\rm cool}(T_{\rm RI} - T_{\rm RO}) \tag{A.1}$$

where $T_{\rm RI}$ and $T_{\rm RO}$ are the radiator coolant inlet and outlet temperatures (see Fig. 3) which can be measured by thermocouple sensors. The variable $\dot{m}_c$ is the coolant mass flow rate listed in Table I. The heat transfer efficiency, ε, is calculated

TABLE BII
AIR SPEED RECORDINGS FOR FANS NO. 1 AND NO. 2 OPERATING AT 2000 R/MIN

	Air Speed, $v_{\rm air^*_i}$,(m/s)					
Vertical and Horizontal Points	1	2	3	4	5	Ave.
1	3.18	2.72	1.81	3.18	2.72	2.72
2	0.57	2.84	2.61	1.36	2.04	1.88
3	1.70	1.25	1.25	1.82	1.02	1.41
4	0.57	0.57	0.57	0.45	0.68	0.57
5	0.79	0.68	0.57	0.57	1.02	0.73
6	0.79	0.91	0.45	0.45	0.91	0.70
Ave.	1.27	1.49	1.21	1.30	1.40	1.33

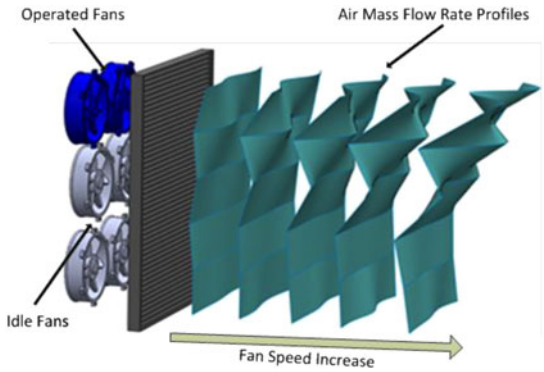

Fig. B.2. Air mass flow rate profiles, $\dot{m}^*_{\rm air}$, for increasing fan speeds, $1000 < N < 5000$ (r/min), with no. 1 and no. 2 fans operating.

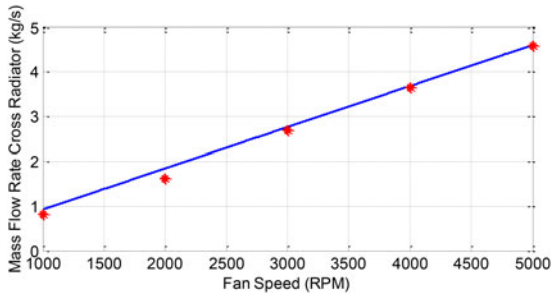

Fig. B.3. Air mass flow rate,$m_{\rm air}$, versus fan speed, N, with no. 1 and no. 2 fans operational for both the mathematical model (blue line) and the experimental test (red scatters).

based on (3) with $\varepsilon = \frac{q_{\rm out}}{\dot{m}_{\rm air} C p_{\rm air}(T_{a\rm out} - T_{a\rm in})}$ where the air specific heat, $Cp_{\rm air}$, and $\Delta T = T_{a\rm out} - T_{a\rm in}$ are summarized in Table I. The curve of the heat transfer efficiency, ε, versus the different mass air flow rates, $\dot{m}_{\rm air}$, based on tests result is represented in Fig. A.1. Using the Matlab curve fitting tool, a quadratic equation $\varepsilon = a\dot{m}^2_{\rm air} + b\dot{m}_{\rm air} + c$ was fitted.

The efficiency, η, is calculated based on (10) with $\eta = \frac{2\pi k}{60 P_e} N^3$ where the factor k is listed in Table I. Through experimental testing, the fan speed, N, and the fan power, P_e, were recorded and summarized in Table AII. The fan power consumption, P_e, was calculated as the average value for Test VI as listed in Table II. Fig. A.2 shows the trend curve of the fan speed versus efficiency. A second-order curve fitting was

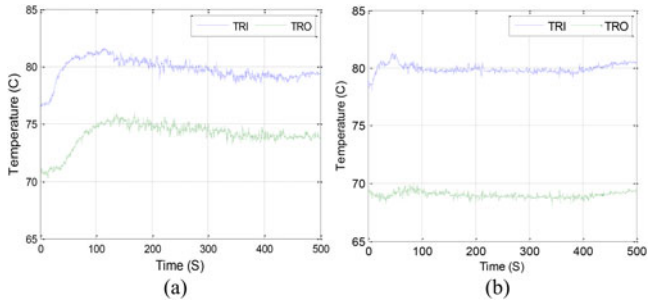

Fig. B.4. Temperature of radiator inlet, T_{RI}, and outlet, T_{RO}, when the fan speed is (a) 2000 and (b) 5000 r/min.

TABLE BIII
COOLANT TEMPERATURE AND HEAT REJECTED CALCULATION RESULTS FOR FANS NO. 1 AND NO. 2 OPERATING AT VARIOUS SPEED

Fan Speed, *N* (r/min)	1000	2000	3000	4000	5000
Radiator Inlet, T_{RI}, (°C)	80.1	79.9	80.4	81.0	80.2
Radiator Outlet, T_{Ro}, (°C)	76.5	74.7	72.7	72.3	68.8
Heat Rejected, q_{out}, (kW)	17.3	25.0	37.0	41.8	54.8

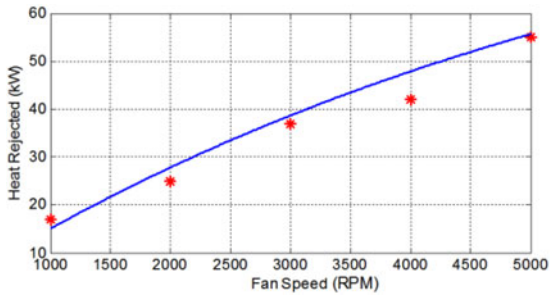

Fig. B.5. Heat rejected from radiator,q_{out}, versus fan speed, *N*, with no. 1 and no. 2 fans operational for both the mathematical model (blue line) and the experimental test (red scatters).

selected with $\eta = dN^2 + eN + f$ to determine the relationship between the fan speed, *N*, and efficiency, η.

APPENDIX B

A series of experimental tests were performed on the cooling system to validate the mathematical models proposed in Sections II and III. The specific test results considered include: 1) radiator air mass flow rate, m_{air}, 2) heat rejected from the radiator, q_{out}, and 3) fan matrix power consumption,P_e, for different fan speeds,N, and number of fans, n. To demonstrate the versatility of the dynamic models, two fans (no. 1 and no. 2) were selected for operation. The test profile and the corresponding results are listed in Table BI. As demonstrated through laboratory testing, the mathematical model adequately estimates the system behavior.

A. Radiator Air Mass Flow Rate Model Validation

The relationship between the fan configuration (e.g., fan speed, N, and number of fans, n) and the air mass flow rate through the radiator, m_{air}, can be expressed as

$$m_{\mathrm{air}} = \frac{4\pi^2 \rho_{\mathrm{air}} r_m^3 \Phi_m N n}{60} \left(\frac{1-v^2}{1+v^2}\right) \sqrt{\frac{K_f}{K_r}} \tag{B1}$$

when there is this no ram air effect, $\dot{m}_{\mathrm{ram}} = 0$, from (7) and (15). Alternatively, the radiator air mass flow rate, $\dot{m}_{\mathrm{air}}$, can be experimentally determined by measuring the air speed exiting the radiator,v^*_{air}, and introducing some system parameters into the corresponding basic engineering calculations. Thirty points were marked on the radiator as shown in Fig. B.1 to establish a grid and data collected for different fan rotational speeds, N. The average air flow speed, $\bar{v}^*_{\mathrm{air}}$, was calculated based on the collected wind speed data to obtain the total air mass flow rate, $\dot{m}^*_{\mathrm{air}}$, through the radiator area.

For example, the air flow speed, $v^{*_i}_{\mathrm{air}}$ $(i = 1, 2, \ldots, 30)$, at each point with a fan speed of $N = 2000$ r/min has been listed in Table BII. In these tests, the average air speed cross the radiator is $\bar{v}^*_{\mathrm{air}} = 1.33$ m/s, and the testing mass flow rate, $\dot{m}^*_{\mathrm{air}}$, can be calculated using (4) as $\dot{m}^*_{\mathrm{air}} = \bar{v}^*_{\mathrm{air}} A_r \rho_{\mathrm{air}} = 1.61$ kg/s.

The three-dimensional surfaces corresponding to the measured air mass flow rate profile, $\dot{m}^*_{\mathrm{air}}$, for increasing fan speed are displayed in Fig. B.2. The calculated air mass flow rate using the mathematical model and the test data are summarized in Fig. B.3 and Table BI. The average absolute error between the mathematical model and the experimental results is 6.2%.

TABLE BIV
CURRENT AND POWER FOR NO. 1 AND NO. 2 FANS OPERATION AT $V_s = 30$ V

Fan Speed, *N* (r/min)	1000	2000	3000	4000	5000
Test Current, i (A)	3.3	6.4	10.9	19.8	35.0
Test Fan Power, $P_e = iV_s$ (kW)	0.10	0.19	0.33	0.60	1.05

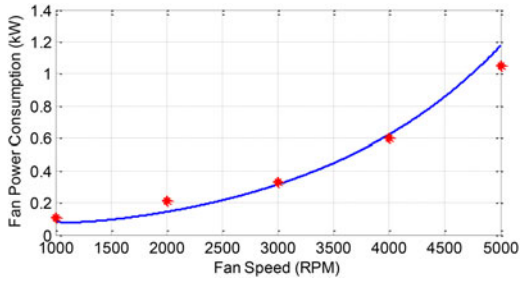

Fig. B.6. Fan power consumption,P_e, versus fan speed, *N*, versus fan speed, *N*, with no. 1 and no. 2 fans operational for both the mathematical model (blue line) and the experimental test (red scatters).

B. Heat Rejected From Radiator Model Validation

The radiator heat rejection, q_{out}, will be validated as described by (19). As stated in (A1), the coolant's thermal response can be used as an alternative representation of the heat rejection from the radiator, q_{out}, provided that the system has reached equilibrium. Each test was operated for a 500-s time period and the temperatures at steady state are selected to calculate the heat output. Fig. B.4 presents the coolant temperature at the radiator

inlet, $T_{\rm RI}$, and outlet, $T_{\rm RO}$, when the twin radiator fans are operated at 2000 and 5000 r/min, respectively. For example, when the fans spin at 2000 r/min, the temperature at the radiator inlet is $T_{\rm RI} = 79.9\ ^{\circ}{\rm C}$ while at the outlet $T_{Ro} = 74.7\ ^{\circ}{\rm C}$. According to (A1), the heat rejection from the radiator is $q_{\rm out} = 25.0\ {\rm kW}$. In comparison, the numerical result from the mathematical model of (19) is calculated as $q_{\rm out} = 27.8\ {\rm kW}$. The test results for all cases are listed in Table BIII. The summarized experimental and numerical results are presented in Fig. B.5 and Table BI; the average absolute error is 8.9%.

C. Radiator Fan Power Consumption Model Validation

To investigate the accuracy of (13), the operating current of the radiator fans has been measured during the test matrix. The supply voltage is fixed at $V_s = 30$ V. The recorded current, i, and the calculated power consumption, $P_e = iV_s$, are listed in Table BIV. The summarized results are listed in Table BI and Fig. B.6 to compare with the mathematical model. The average absolute error is 11.9%.

REFERENCES

[1] F. Melzer, U. Hesse, G. Rocklage, and M. Schmitt, "Thermomanagement," presented at the SAE World Congr., Detroit, MI, USA, Mar. 1999, Paper 1999-01-0238.

[2] J. Chastain, J. Wagner, and J. Eberth, "Advanced cooling components, testing and observations," in *Proc. 6th IFAC Symp. Adv. Automotive Control*, Jul. 2010, pp. 294–299.

[3] J. Heywood, *Internal Combustion Engine Fundamentals*. New York, NY, USA: McGraw-Hill, 1988.

[4] T. Mitchell, M. Salah, J. Wagner, and D. Dawson, "Automotive thermal valve configurations: Enhanced warm-up performance," *ASME J. Dyn. Syst., Meas. Control*, vol. 131, no. 4, pp. 239–244, Jul. 2009.

[5] M. Chanfreau, B. Gessier, A. Farkh, and P. Geels, "The need for an electrical water valve in a thermal management intelligent system (THEMIS)," presented at the SAE World Congr., Detroit, MI, USA, Mar. 2003, Paper 2003-01-0274.

[6] J. Wagner, M. Ghone, and D. Dawson, "Cooling flow control strategy for automotive thermal management systems," presented at the SAE World Congr., Detroit, MI, USA, Mar. 2002, Paper 2002-01-0713.

[7] R. Page, W. Hnatczuk, and J. Kozierowski, "Thermal management for the 21st century—Improved thermal control and fuel economy in an army medium tactical vehicle," presented at the Vehicle Thermal Management Systems Conf. Expo., Toronto, Canada, May 2005, Paper 2005-01-2068.

[8] R. Badekar, J. Mahajan, S. Kakaye, P. Khire, and K. Gopalkrishna, "Development of control system for electrical radiator fan using dual sensor and microprocessor based electronic unit," presented at the SAE World Congr., Detroit, MI, USA, Apr. 2006, Paper 2006-01-1035.

[9] M. Salah, T. Mitchell, J. Wagner, and D. Dawson, "An advanced engine thermal management system: Nonlinear control and test," *IEEE Trans. Mechatron.*, vol. 10, no. 2, pp. 210–220, Apr. 2005.

[10] M. Salah, T. Mitchell, J. Wagner, and D. Dawson, "A smart multiple loop automotive cooling system model, control, and experimental study," *IEEE Trans. Mechatron.*, vol. 15, no. 1, pp. 117–124, Feb. 2010.

[11] K. Choi, H. Kim, W. Cho, and K. Lee, "Investigation of emission reduction effect by controlling cooling system in a diesel engine," presented at the Power Strain Fluid System Conf. Exhib., Chicago, IL, USA, Oct. 2007, Paper 2007-01-4064.

[12] F. Regin, "A numerical analysis on air-cooling performance of passenger cars," presented at the SAE World Congr., Detroit, MI, USA, Apr. 2010, Paper 2010-01-0554.

[13] P. Dube, S. Natarajan, A. Mulemane, and V. Damodaran, "A numerical approach to develop the front end cooling package in a vehicle using predicted engine fan performance data and vehicle system resistances," presented at the SAE World Congr., Detroit, MI, USA, Apr. 2007, Paper 2007-01-0542.

[14] T. Fukano and C. Jang, "Tip clearance noise of axial flow fans operating at design and off-design condition," *J. Sound Vibration*, vol. 275, no. 3–5, pp. 1027–1050, 2004.

[15] C. Taylor and T. Toong, "Heat transfer in internal-combustion engine," presented at the ASME-AiChE Heat Transfer Conf., University Park, PA, USA, Aug. 1957, Paper 295.

[16] B. Shome and R. Joshi, "CFD based air-to-boil temperature prediction for sport utility vehicle radiator," presented at the SAE Powertrain Fluid Systems Conf. Exhib., Toronto, Canada, Oct. 2006, Paper 2006-01-3266.

[17] A. Lelkes and M. Bufe, "BLDC motor for fan application with automatically optimized commutation angle," in *Proc. 35th Annu. IEEE Power Electron. Spec. Conf.*, Jun. 2004, pp. 2277–2281.

[18] R. Jorgensen, *Fan Engineering*. Buffalo, NY, USA: Buffalo Forge Company, 1982.

[19] R. H. Byrd, M. E. Hribar, and J. Nocedal, "An interior point algorithm for large-scale nonlinear programming," *SIAM J. Optimization*, vol. 9, no. 4, pp. 877–900, 1999.

[20] M. C. Biggs, "Constrained minimization using recursive quadratic programming," in *Towards Global Optimization*. Amsterdam, The Netherlands: North Holland, 1975, pp. 341–349.

[21] D. Moyle, M. Lasecki, and B. Cornish, "Thermal kits for truck fleets," presented at the SAE Commercial Vehicle Engineering Congr., Chicago, IL, USA, Oct. 2006, Paper 2006-1-3542.

Tianwei (Thomas) Wang received the B.S. and M.S. degrees in mechanical engineering from the East China University of Science and Technology, Shanghai, China, in 2011. He is currently working toward the Ph.D. degree at the Mechanical Engineering Department, Clemson University, Clemson, SC, USA.

His research interests include nonlinear and intelligent control theory, automotive cooling system, and 3-D visualization engineering education.

Amit Jagarwal received the B.E. degree from Pune University, Pune, India, in 2005, and the M.E. degree from Clemson University, Clemson, SC, USA, in 2010.

He has held several design and engineering positions at TATA Motors, Larsen & Toubro, TATA Technologies and Lang-Mekra over the past years. Since 2011, he is a Senior Product Engineer at TRW Automotive Inc., North America, working on product development activities for electrically powered steering systems division. His research interests include product modeling, analysis and prototype testing.

John R. Wagner (SM'11) received the B.S., M.S., and Ph.D. degrees in mechanical engineering from the State University of New York, Buffalo, NY, USA, and Purdue University, West Lafayette, IN, USA.

He is currently a Professor at the Mechanical Engineering Department, Clemson University, Clemson, SC, USA. He was previously on the engineering staff at Delco Electronics and Delphi Automotive Systems designing automotive control systems. His research interests include nonlinear and intelligent control theory, diagnostic and prognostic strategies, automotive safety, and mechatronic system design. He has established the multidisciplinary Automotive and Mechatronics Research Laboratory and the Rockwell Automation Mechatronics Educational Laboratory at Clemson University.

Dr. Wagner is a Licensed Professional Engineer and a Fellow of the American Society of Mechanical Engineers.

Georges Fadel received the Diploma in mechanical engineering from ETH Zurich, Zurich, Switzerland, and the M.S. degree in computer science and the Ph.D. degree in mechanical engineering from Georgia Tech, Atlanta, GA, USA.

He is currently the Professor and Exxon Mobil Employees Chair in mechanical engineering at Clemson University, Clemson, SC, USA. His research interests include packaging or layout optimization, material by design, additive manufacturing, and design theory (affordances). He has published more than two hundred refereed research articles.

Dr. Fadel is a Fellow of the American Society of Mechanical Engineers, and past chair of its TC on design automation, Member of AIAA, SAE, ISSMO, and MCDM, and of the Board of Management of the Design Society.